Wear 268 (2010) 335–345

Contents lists available at ScienceDirect

Wear

journal homepage: www.elsevier.com/locate/wear

An experimental study on roughness noise of dry rough flat surfaces

H. Ben Abdelounis*, A. Le Bot, J. Perret-Liaudet, H. Zahouani

Laboratoire de Tribologie et Dynamique des Systèmes, UMR 5513, École Centrale de Lyon, 36 avenue Guy de Collongue, 69134 Écully Cedex, France

ARTICLE INFO

Article history:
Received 14 October 2008
Received in revised form 20 June 2009
Accepted 12 August 2009
Available online 22 August 2009

Keywords:
Friction
Noise
Vibration
Roughness
Contact
Sliding
Topography

ABSTRACT

This paper presents an experimental study of the friction noise, between two rough and dry flat surfaces. The domain of interest is the dry contact under light pressure where the roughness is the dominant cause of noise. The results show that, for sliding rough surfaces under light load, the fundamental mechanism of radiated noise is the presence of shocks occurring between antagonist asperities of sliding surfaces. The radiated roughness noise is controlled simultaneously by the detailed topography of the surfaces in contact, the sliding speed and the dynamics of the surfaces. In terms of topography and sliding speed, it was shown that the roughness noise is simultaneously an increasing linear function of the logarithm of the surface roughness and the sliding speed. In terms of dynamics, the roughness noise is generated for light dynamical coupling. Hence, the natural modes of samples are stiffer than the contact and therefore the resulting vibrations are not affected by the additional rigidity. The deformation of surfaces during contact is very light and its magnitude is negligible compared to the surface roughness.

1. Introduction

The dynamics of rough contact can be tackled by three different approaches: the tribological approach, the structural dynamics approach and the acoustical approach. The tribological approach generally focuses on the surface topography and its role on the determination of the tribological behaviour of the surfaces [1–4]. The structural dynamics approach has an interest in the study of friction-induced vibrations and its consequence on the friction itself [5–9]. The acoustical approach is reserved to the friction noise study [10–21].

Friction noise may be classified in two categories according to the contact pressure level between the sliding solids [20]. When the contact pressure is high, the friction noise stems from mechanical instabilities such as sprag-slip, stick-slip. Some examples of such a noise are break squeal or squeak of doors. These instabilities can emerge even with perfectly flat surfaces. The physical condition to generate instabilities is generally related with a kinetic friction coefficient at a lower level than the static friction coefficient. On the other hand, when the contact pressure is low, the friction noise is called roughness noise [20] meaning that roughness plays a crucial role. The coupling between the two solids in contact is weak and the eigenfrequencies of isolated solids are not affected by the contact. Under these conditions, the radiated noise is attributed to the numerous impacts between the antagonist asperities of sliding surfaces.

In the literature, the noise due to the mechanical instabilities was largely studied. But, the roughness noise has not received a so great attention, and its phenomenology is not yet fully explained. Some experimental studies have proposed a relationship between the sound pressure level Lp (dB) and the friction parameters such as the surface roughness and the sliding speed. It is to be noted that all these studies were realized either at a constant sliding speed or a constant surface roughness. Unfortunately, the obtained results vary from a study to another. Thus, Takahashi [10] found, for a cylinder-flat contact, and a constant sliding speed, that the sound pressure level Lp (dB) is an increasing function of the surface roughness according to the following logarithmic law:

$$Lp\ (\mathrm{dB}) \sim 20 \log_{10} Ra^{n} \tag{1}$$

with $n = 1$. Nakai and Yokoi [15] have shown that $0.8 \leq n \leq 1.2$ for the same relationship and for a pin-flat contact and constant sliding speed. But, using a stylus-flat contact, Othman et al. [17,18] have found that $0.25 \leq n \leq 0.64$ which is lower than the previous values.

The flat–flat contact was studied for the first time by Stoimenov et al. [21]. They observe that the evolution of the sound pressure level versus surface roughness is in agreement with previous observations on concentrated contacts. Lp (dB) verifies Eq. (1) with $0.7 \leq n \leq 0.85$.

Concerning the dependence of Lp (dB) with the sliding speed, Nakai and Yokoi [15] showed that Lp (dB) is also a logarithmic

* Corresponding author at: Ecole Centrale de Lyon, Laboratoire de Tribologie et Dynamique des Systèmes – Bat H10, 36 avenue Guy de Collongue, 69130 Ecully, France. Tel.: +33 472186294; fax: +33 478433383.
E-mail address: houcine.ben-abdelounis@ec-lyon.fr (H. Ben Abdelounis).

0043-1648/$ – see front matter © 2009 Elsevier B.V. All rights reserved.
doi:10.1016/j.wear.2009.08.024

function

$$Lp\,(\mathrm{dB}) \sim 20\log_{10} V^m \tag{2}$$

where the slope m varies between 0.6 and 1.1.

In this paper, we consider the empirical laws for a flat–flat contact of the sound pressure level Lp (dB) by considering simultaneously surface roughness and sliding speed to extent previous results. In particular, one of objectives is to clarify if the sound pressure level may be put into the following relationship:

$$Lp\,(\mathrm{dB}) \sim 20\log_{10} Ra^n V^m \tag{3}$$

with n and m are two independent exponents.

This paper is organized as follows. Following this section, in Section 2 is presented the experimental set-up. In Section 3 is presented the experimental results. Discussion and comments are presented in Section 4. Finally in Section 5, this paper is concluded.

2. Experimental test set-up

The experiment consists to rub two samples with rough surfaces and to record the friction noise radiated in a quasi-anechoic chamber. Rubbing tests were carried out for dry contact, under light load and with a well controlled sliding speed.

2.1. Mechanical device

The mechanical device is displayed in Fig. 1. It permits a friction configuration, which consists of two rough plane surfaces in contact. The contact system is maintained by a sample holder. This sample holder is placed on a small aperture (170 mm × 68 mm) on the face of a small quasi-anechoic chamber. It is decoupled from the chamber by an elastomeric joint. It allows the fixing of the lower sample (designated as fixed sample) and the horizontal guidance of the higher one (designated as moving sample). The sample holder is made of polyamide 6.

Table 1
Material properties.

	Steel S235 JRG2	Aluminum AU4G	Brass
Elastic modulus, E (GPa)	210	70	110
Poisson's ratio υ	0.3	0.34	0.35
Density (kg/m^3)	7800	2700	8800
Mass (g)	165	57	186

The moving sample is pulled against the fixed one, with a string, by a quiet DC-motor (type escap 22N28).

The parallelepipedic quasi-anechoic chamber (700 mm × 580 mm × 570 mm) is built in wood panels, which have 18 mm thickness, covered inside by an absorptive material (rock wool) to eliminate acoustical reflections. The thickness of the used absorptive material is 100 mm. To break the symmetry of the interior of the quasi-anechoic chamber, many diffractants panels which have various shapes was added to the inner faces.

2.2. Description of the samples

The rough samples are rectangular plates with size 120 mm × 22 mm. Its thickness is 8 mm. They are made of steel S235JRG2, brass 65 Cu–35 Zn and aluminum AU4G. Table 1 outlines the mechanical characteristics of these materials.

In order to get rough surfaces, the sample surfaces have been prepared by two different techniques, i.e., sandblasting and electrical discharge machining (EDM). Both sandblasting and EDM processes produce random surface roughness.

These measurements have been obtained with a 3D optical profilometer. Fig. 2 shows 3D-surface topography of the samples obtained by sandblasting and by EDM. The topography measurement surface is 2.44 mm × 1.86 mm. The measurement steps are 3.32 μm × 3.87 μm.

In Fig. 3, is shown the height distribution of asperities samples. Table 2 gives the classical surface topography parameters, i.e.,

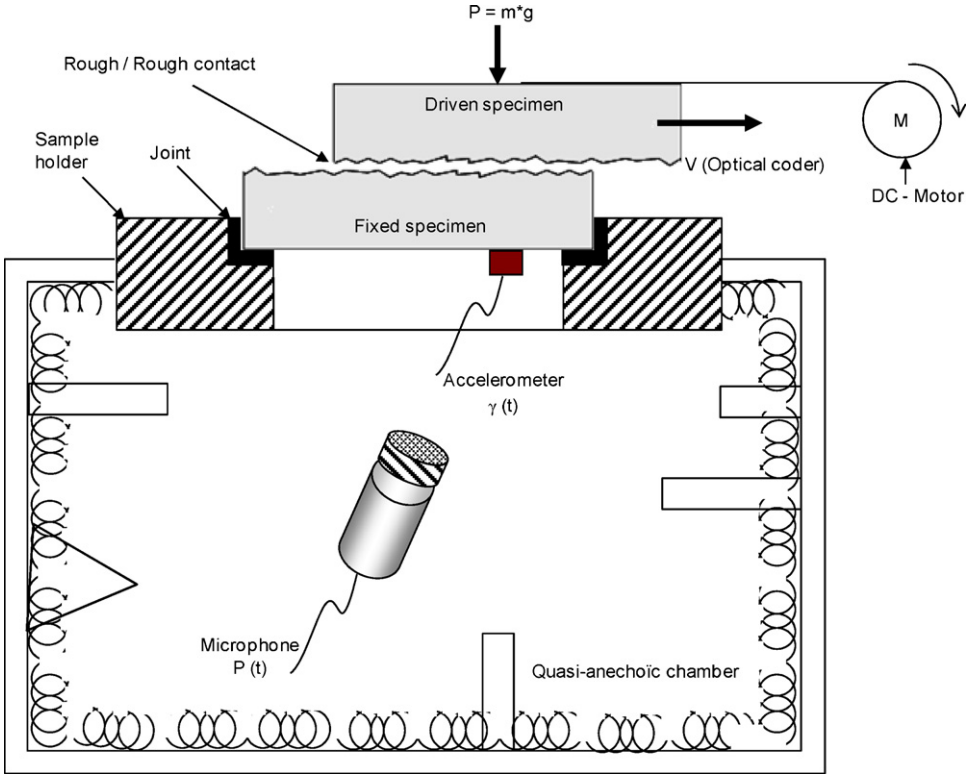

Fig. 1. Experimental apparatus for flat–flat contact.

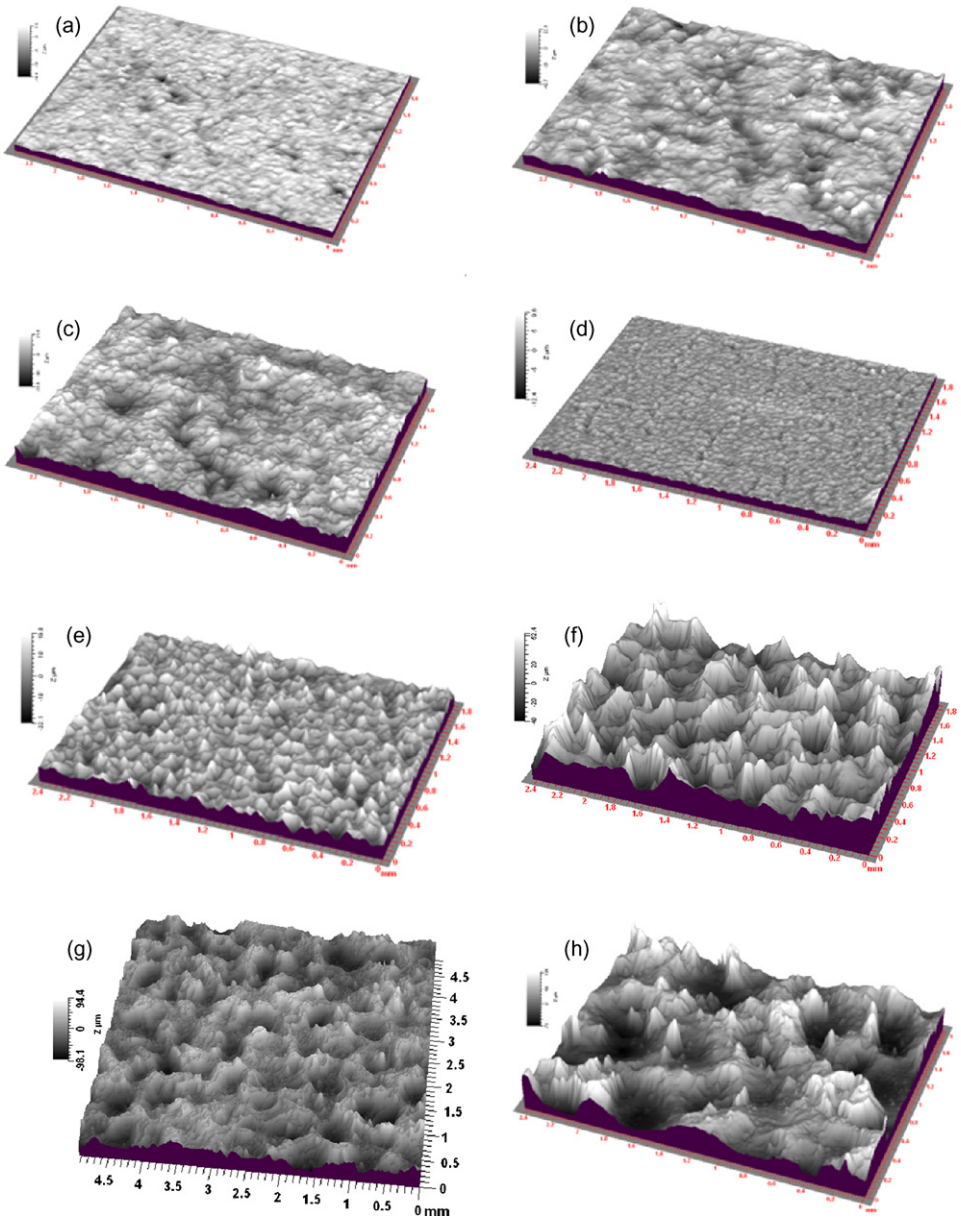

Fig. 2. 3D-surface topography; sandblasting: (a) R_a = 1 μm, (b) R_a = 4 μm, (c) R_a = 5 μm. EDM: (d) R_a = 1 μm, (e) R_a = 4.5 μm, (f) R_a = 10 μm, (g) R_a = 20 μm, (h) R_a = 26 μm.

the arithmetic surface roughness R_a, the skewness of topography height distribution *Sk* and the kurtosis of topography height distribution *Ek*. Furthermore, the asperities spacing *Rsm*, the average radius of the peaks R_{moy}, the standard deviation of the asperities heights distribution σ and the peaks' number *N* by 4.53 mm^2.

2.3. Instrumentation and acquisition

An optical coder, type Renishaw RGH22 D30D00 measures the displacement of the driven sample. The optical head is mounted on the sample holder and the scale is sticked on the moving sam-

Table 2
Surface roughness and topography parameters obtained by profilometer for sandblasting and EDM. R_a is the arithmetic surface roughness, *Sk* and *Ek* are respectively the Skewness and the Kurtosis of the topography height distribution, *Rsm* is the asperities spacing, R_{moy} is the average radius of the peaks, σ is the standard deviation of the asperities heights distribution, *N* is the peaks number by 4.53 mm^2.

	Sandblasting			EDM				
R_a (μm)	1	4	5	1	4.5	10	20	26
Sk	−1.1	−0.41	−0.53	−0.07	−0.03	0.17	0.25	0
Ek	5.7	3.55	3.19	3.1	3.15	2.96	2.9	2.83
Rsm (μm)	79	160	173	92	150	276	410	516
R_{moy} (μm)	119	45	40	64	57	52	30	12
σ (μm)	1.83	6.45	7.74	1.1	4.1	10	13	8.62
N	3792	2845	2380	6559	2079	1974	1000	934

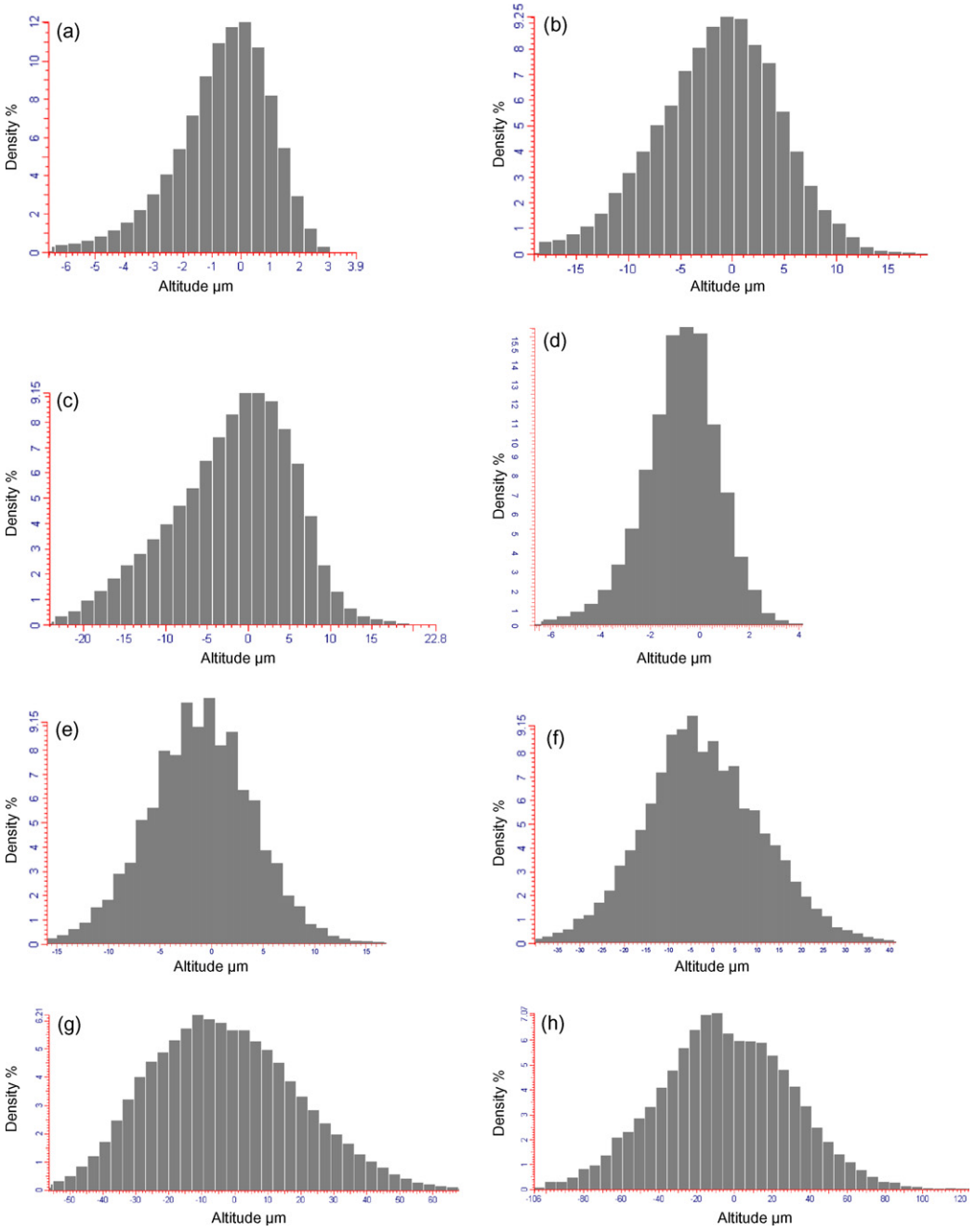

Fig. 3. Distribution heights of asperities; sandblasting: (a) $R_a = 1$ µm, (b) $R_a = 4$ µm, (c) $R_a = 5$ µm. EDM: (d) $R_a = 1$ µm, (e) $R_a = 4.5$ µm, (f) $R_a = 10$ µm, (g) $R_a = 20$ µm, (h) $R_a = 26$ µm.

ple. The coder sensitivity is 5 µm. The sliding speed is obtained by a numerical derivative of the displacement (finite difference method). The friction noise inside the quasi-anechoic chamber is recorded by a B&K ½ in. microphone type 4189-L-001. The microphone sensitivity is 46.9 mV/Pa, and its frequency ranges from 6 Hz to 20 kHz. The microphone is placed at about 670 mm below the rubbed samples. A B&K 1/4 in. microphone having a large frequency range (6 Hz–100 kHz) is used to measure the total friction noise signal.

A B&K accelerometer type 4517-C-001 is mounted on the lower face of the fixed sample to measure the vibrational acceleration. The accelerometer sensitivity is 0.1974 pc ms^{-2} and the frequency band is 5 Hz–20 kHz. Its weight is 10^{-3} kg.

All these signals are acquired simultaneously on a computer, by a digital I/O board PCI-DAS-6013 16 bits.

As we are only interested in audible noise, all measurements of this study were confined into the audio band 20 Hz–20 kHz by using an anti-aliasing filter. The sampling frequency is 48 kHz. Power spectrum densities are obtained with 4096 lines and a Hanning time window.

2.4. Dynamical characteristics of the samples

In order to determine the modal properties of the samples a numerical dynamic model based on the finite element method is built. The volume is meshed by 6325 tetrahedral volume elements, 4 nodes per element, resulting in 10,581 nodes. The behaviour law of the elements is the classical linear elasticity. Free boundary conditions are chosen for the finite element model.

The obtained first eigenfrequencies are given in Table 3.

Table 3
Numerical eigenfrequencies (Hz) of the samples.

	f1	f2	f3	f4	f5	f6	f7
Num. value (Hz)	2920	7354	7854	8086	14902	16351	17649

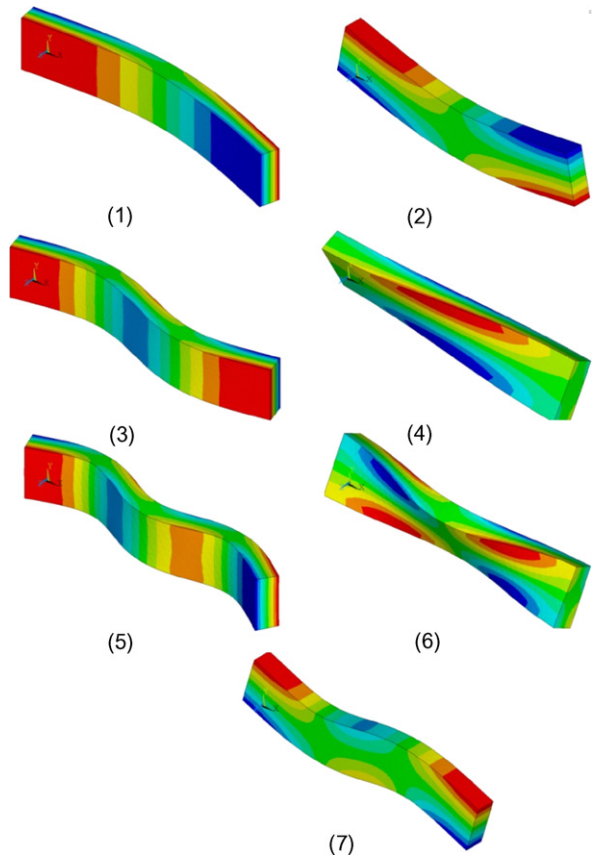

Fig. 4. Eigenmodes of the isolated samples by finite element method. (1) First flexural mode (2920 Hz). (2) First transverse flexural mode (7354 Hz). (3) Second flexural mode (7854 Hz). (4) First torsional mode (8086 Hz). (5) Third flexural mode (14902 Hz). (6) Second torsional mode (16351 Hz). (7) Second transverse flexural mode (17649 Hz).

As we can see, only seven eigenmodes take place on the frequency audio band. The associated eigenvectors are shown in Fig. 4. We can observe five modes which can radiate noise in the quasi-anechoic chamber, i.e., three modes associated to flexural motion (nos. 1, 3 and 5), and two modes associated to torsional motion (no. 4 and 6). The other two eigenmodes (no. 2 and 7) are characterized by in plane motion.

To validate the numerical results, frequency response function (FRF) is performed. For this, sample is suspended and excited by a shaker. The measured experimental eigenfrequencies and the corresponding modal damping factors are given in Table 4. As one can see, numerical eigenfrequencies agree with well the experimental ones.

Table 4
Experimental eigenfrequencies and modal damping factors of the samples.

	Exp. eigenfrequencies (Hz)	Exp. modal damping factor
f1	2900	0.02
f2	7400	0.005
f3	7900	0.004
f4	8100	0.004
f5	14500	0.009
f6	16500	0.009
f7	17500	0.004

Table 5
Experimental eigenfrequencies and modal damping factors of the sample holder.

	Exp. eigenfrequencies (Hz)	Exp. modal damping factor
f1	850	0.016
f2	1975	0.01
f3	4050	0.013
f4	5300	0.01
f5	16190	0.01

Table 6
Numerical eigenfrequencies of the sample holder.

	f1	f2	f3	f4	f5
Num. value (Hz)	843	2000	3850	5376	16111

The same analysis is performed for the sample holder with free boundary conditions. The experimental eigenfrequencies are shown in Table 5. From a finite element model (45,554 tetrahedral volume elements and 9884 nodes), we have found several modes which confirm these experimental ones (Table 6).

As the eigenmodes of the samples and the sample holder are in the same range of frequency, we have uncoupled the fixed sample from the sample holder by adding a soft synthetic rubber joint between them.

2.5. Contact stiffness and its effects on the modal properties of samples

In the case of the two rough plane surfaces, the contact stiffness can be estimated from the Greenwood and Williamson model [22]. It is considered that the two nominally flat surfaces, in contact, are respectively covered with a large number of spherically tipped asperities with same radius β_1 and β_2, and randomly distributed heights described by a probability density function $\Phi(z)$. From this model, the expected load W is expressed by

$$W = \frac{4}{3} N E' \beta^{1/2} \int_d^{\infty} (z-d)^{3/2} \phi(z) dz \quad (4)$$

where N is the number of the all surface asperities, E' is the reduced elasticity modulus such as $1/E' = (1-\upsilon_1^2)/E_1 + (1-\upsilon_2^2)/E_2$, β is the equivalent radius such as $1/\beta = 1/\beta_1 + 1/\beta_2$, z is the asperity height and d is the separation between the two sliding surfaces in contact.

As an example, Fig. 5 shows the evolution of the load versus the relative displacement for the case of the EDM sample with $R_a = 26\,\mu m$.

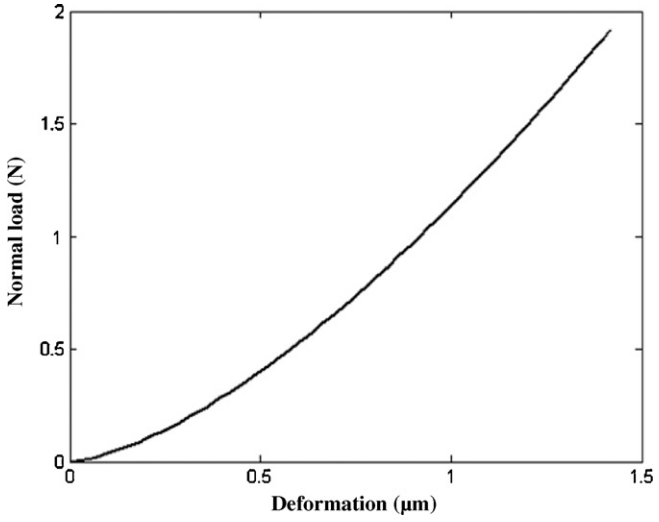

Fig. 5. Variation of the normal load versus the relative deformation for $R_a = 26\,\mu m$.

Table 7
Contact stiffness $K_{G\&W}$ (N/μm) estimated from Greenwood and Williamson modelling, expected number of contact (N_c) and real contact area (mm²) for R_a = 1 μm, 4.5 μm, 10 μm, 20 μm and 26 μm and under 1.62 N applied normal load.

	R_a (μm) (by EDM)				
	1	4.5	10	20	26
$K_{G\&W}$ (N/μm)	6	3.6	3	2.5	1.92
N_c	1689	324	165	59	3
A_r (mm²)	406	72	35	9	0.24

The normal contact stiffness $K_{G\&W}$ is defined by linearising Eq. (4) around the static load W_s:

$$K_{G\&W} = \frac{\partial W}{\partial \delta} \mid = 2NE'\beta^{1/2} \int_d^{\infty} (z-d)^{1/2} \phi(z)\, dz \quad (5)$$

where $\delta = z - d$.

In this study, W_s corresponds to the weight of the driven sample and it is equal to 1.62 N. The estimated contact stiffness versus surface roughness, for this static load is given in Table 7. It is given also in Table 6 the number of contact points N_c and the real contact area A_r. It is to be noted here that, in view of the asperities heights distribution, only one contact point is observed for R_a = 26 μm. But, for two solids to be in equilibrium, at least three contact points should be considered (Table 7).

From this table, is clearly seen that the contact stiffness is negligible compared to the elastic properties of the used samples. The number of contact points and the real contact area decrease when the surface roughness increases. It means that the coupling between the two samples is light and that the samples behave like being totally uncoupled.

2.6. Acoustic properties of the quasi-anechoic chamber

The sound insulation of the quasi-anechoic chamber was measured by generated Gaussian noise. The sound pressure level Lp (dB) is measured outside and inside the small quasi-anechoic chamber. In both cases, the position and the distance between the microphone acquisition and the noise source are the same. The distance is fixed at 1 m. The sound pressure level outside ($Lp1$ (dB)) and inside ($Lp2$ (dB)) the quasi-anechoic chamber is 70.3 dB and 39.6 dB, respectively. The sound insulation D (dB) is then equal to $Lp1 - Lp2$ = 30.7 dB.

The acoustical eigenmodes of the quasi-anechoic chamber are identified in an experimental way. Fig. 6 shows the frequency response function (FRF) between the acoustical pressure measured with a microphone and a voltage across a loudspeaker. Both microphone and loudspeaker are positioned inside the quasi-anechoic chamber. This FRF is realized with a white noise excitation within the audio band. The corresponding transfer function coherence is shown in Fig. 7. Five main eigenmodes have been observed in the audio band. The experimental eigenfrequencies are given in Table 8.

Table 8
Experimental acoustical modes of the quasi-anechoic chamber.

	Exp. eigenfrequencies (Hz)	Exp. modal damping factor
f1	1300	0.23
f2	2088	0.10
f3	3900	0.03
f4	5100	0.04
f5	5600	0.03

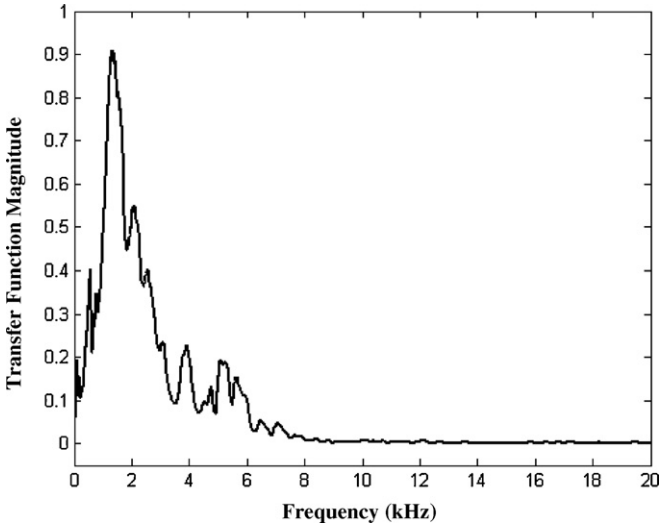

Fig. 6. Measured transfer function between a pressure (Pa) and a voltage (V) with a white noise excitation of the anechoic chamber.

2.7. Experimental protocol

Rubbing tests were carried out for samples having same surface roughnesses obtained by the same machining process. Before tests, samples are carefully degreased with acetone. Each friction test is repeated five times. The test is run in ambient atmosphere (relative humidity varied from 73 to 76% and room temperature from 23 to 25 °C). The loading force is just the actual weight of the driven sample (1.62 N). The sliding speed is constant during friction tests and can be varied from 2 to 12 cm/s.

3. Experimental results

3.1. Sound pressure histories and associated spectra

From microphone and accelerometer measurements, we can calculate respectively two physical quantities Lp (dB) and Lv (dB). The sound pressure level Lp (dB) and the vibratory level Lv (dB) are

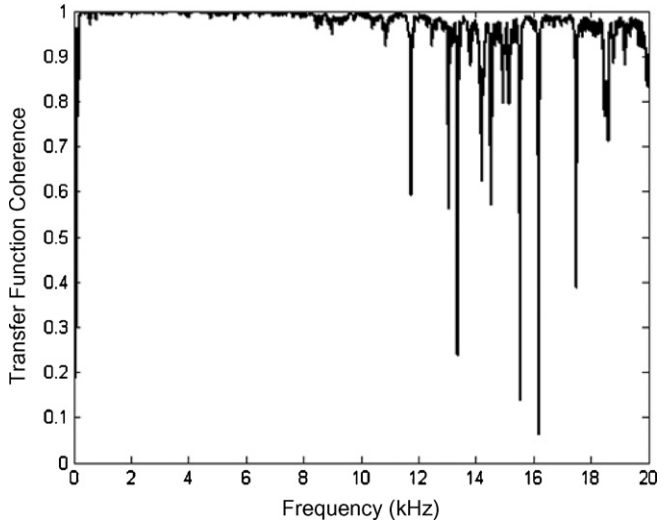

Fig. 7. Transfer function coherence corresponding to the transfer function plotted in Fig. 6.

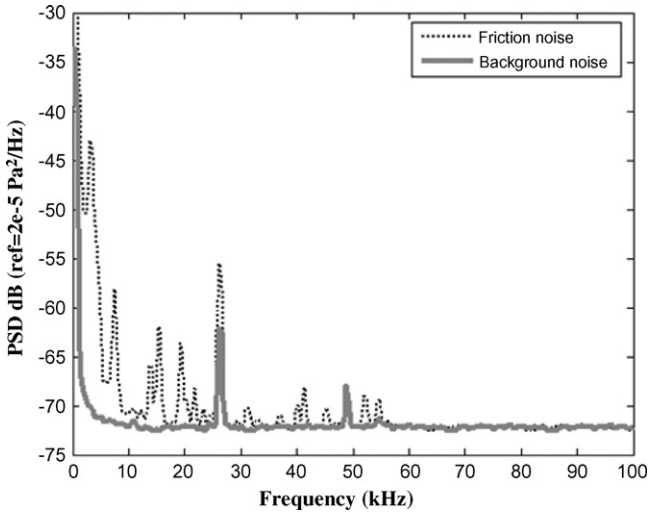

Fig. 8. Spectrum of the roughness noise measured with a 1/4 in. microphone with limiting frequency 70 kHz, sample frequency 200 kHz, R_a = 26 μm obtained by EDM.

obtained from the following relationships:

$$\begin{cases} Lp\ (\text{dB}) = 20\log_{10}\dfrac{P_{eff}}{P_0} \\ Lv\ (\text{dB}) = 20\log_{10}\dfrac{V_{eff}}{V_0} \end{cases} \quad (6)$$

where, $P_0 = 2\times10^{-5}$ Pa, $V_0 = 10^{-8}$ m/s, P_{eff} and V_{eff} are respectively the mean square pressure and the mean square vibratory speed.

The measured friction noise has a very large band spectrum. In Fig. 8, is shown the signal spectrum measured with a 1/4 in. microphone and a high sample frequency (fe = 200 kHz). The noise spectrum is found to extend up to 45 kHz. Beyond this limit, the friction noise level is comparable to the background noise level although the actual friction noise spectrum is certainly wider than it can be measured. As we are only interested in audible roughness noise, all measurements of this study were confined into the audio band 20 Hz–20 kHz by using an anti-aliasing filter.

Our preliminary measurements show that accelerometer or microphone does not modify the variation of the radiated roughness noise versus surface roughness R_a and sliding speed V. In both cases, Lp (dB) and Lv (dB) are linear increasing functions of the logarithm of R_a and V with the same slopes (Fig. 9). The only difference is the offset in the y-axis between Lp (dB) and Lv (dB).

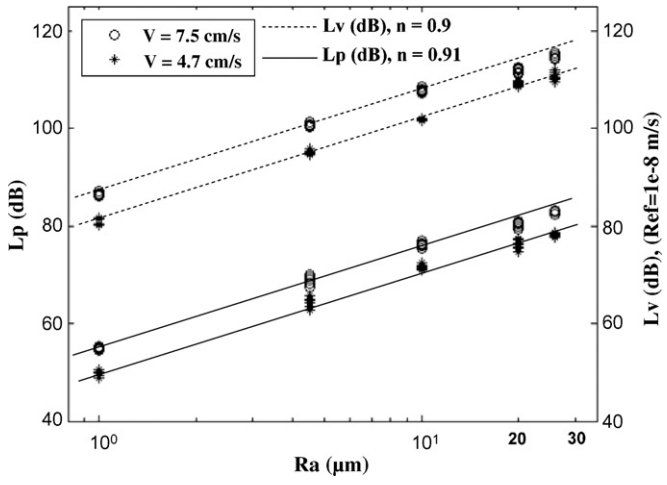

Fig. 9. Comparison between microphone and accelerometer measurements of radiated roughness sound.

However, the accelerometer measurement depends largely on the fixation point of accelerometer on the sample. The vibration is measured in the point where the accelerometer is mounted. Therefore, it is not possible to obtain simultaneously the all eigenmodes of the sample using accelerometer. But, microphone measures the radiated sound through the all sample surface regardless of the excited eigenmodes.

For this reason, only the results obtained by microphone measurements will be presented in this study.

3.2. Sound pressure level versus surface roughness and sliding speed

A typical variation of the sound pressure level Lp (dB) versus the surface roughness and the sliding speed for various materials (steel, brass and aluminum), in the audio band [20 Hz, 20 kHz], is respectively plotted in Figs. 10 and 11. From these figures, it is clearly seen that regardless of the material under investigation, the sound pressure level is an increasing function of the surface roughness and the sliding speed in agreement with Eqs. (1) and (2). It is to be noted here that sound pressure levels at a particular surface roughness or sliding speed are highest for steel, somewhat lower for brass, and lowest for aluminum (Fig. 12). It is interesting to note that steel is stiffer than brass and aluminum is the less stiff one.

The exponents for the laws described in Eqs. (1) and (2) are respectively: $0.7 \le n \le 0.96$ and $0.9 \le m \le 1.16$. These results are in agreement with the observations of Stoimenov et al. [21] for flat–flat contact, but also with the previous studies on concentrated contacts [10–18].

Thus, Stoimenov et al. [21] show, for plate on plate contact, that $0.7 \le n \le 0.85$. Takahashi [10], for a cylinder–flat contact, found that $n = 1$. Nakai and Yokoi [15] have respectively shown that $0.8 \le n \le 1.2$ and $0.6 \le m \le 1.1$ for a pin–flat contact.

From our results and the previous studies, it is clear that the variation of the sound pressure level Lp (dB) versus surface roughness and sliding speed is independent of the contact geometry.

The simultaneously variation of the sound pressure level versus surface roughness and sliding speed for sandblasting and EDM machining process, in the case of steel/steel contact, is shown in Fig. 13. In this figure, is also plotted the fitted data with a linear interpolation. The mean gap between the fitted map and the experimental data is 2.8%.

From these results it is clearly seen that, independently of the samples machining process, Lp (dB) is simultaneously a linear function of the logarithm of the surface roughness and the sliding speed in agreement with Eq. (3). The exponents n and m are independents and they are respectively: $0.71 \le n \le 0.84$ and $0.8 \le m \le 1.1$.

3.3. Contact stiffness

The power spectrum density of friction noise has been measured for different loading forces, roughnesses and sliding speeds. Results are respectively shown in Figs. 14–16. The vertical thick lines point out the position of eigenfrequencies of uncoupled samples computed by finite element method. We first remark that the eigenfrequencies computed by finite element method well match with the peaks of power spectrum density especially for low loading force, high roughness and high sliding speed. It means that the coupling between the two metal pieces is light and that the pieces behave like being totally uncoupled. But when the loading force increases (Fig. 14), when the roughness decreases (Fig. 15) or when the sliding speed decreases (Fig. 16), the coupling become more important and the first eigenfrequency is shifted towards high frequencies. This phenomenon has been pointed out in Ref. [21]. The authors [21] have observed that the peak frequency shifts from

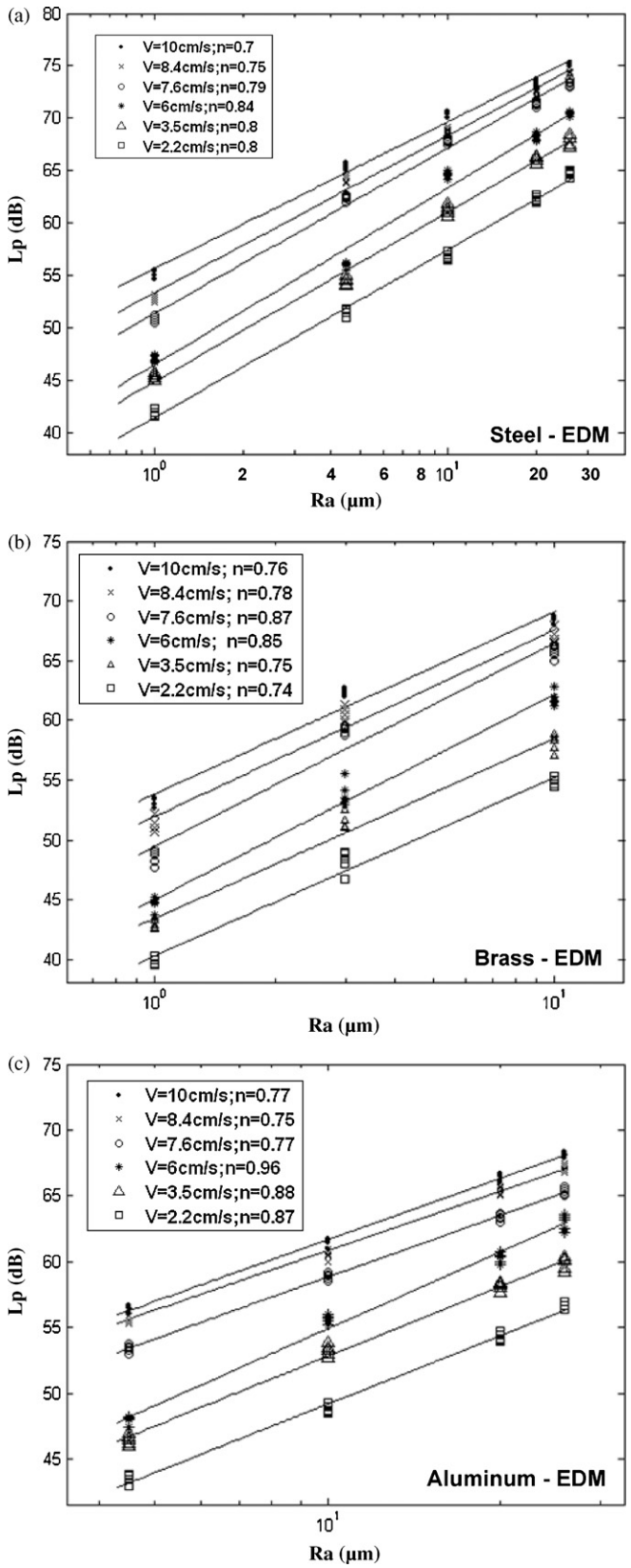

Fig. 10. Variation of the sound pressure level *Lp* (dB) versus the surface roughness, obtained by EDM, for various sliding speeds and different materials. (a) Steel/steel, (b) brass/brass, and (c) aluminum/aluminum.

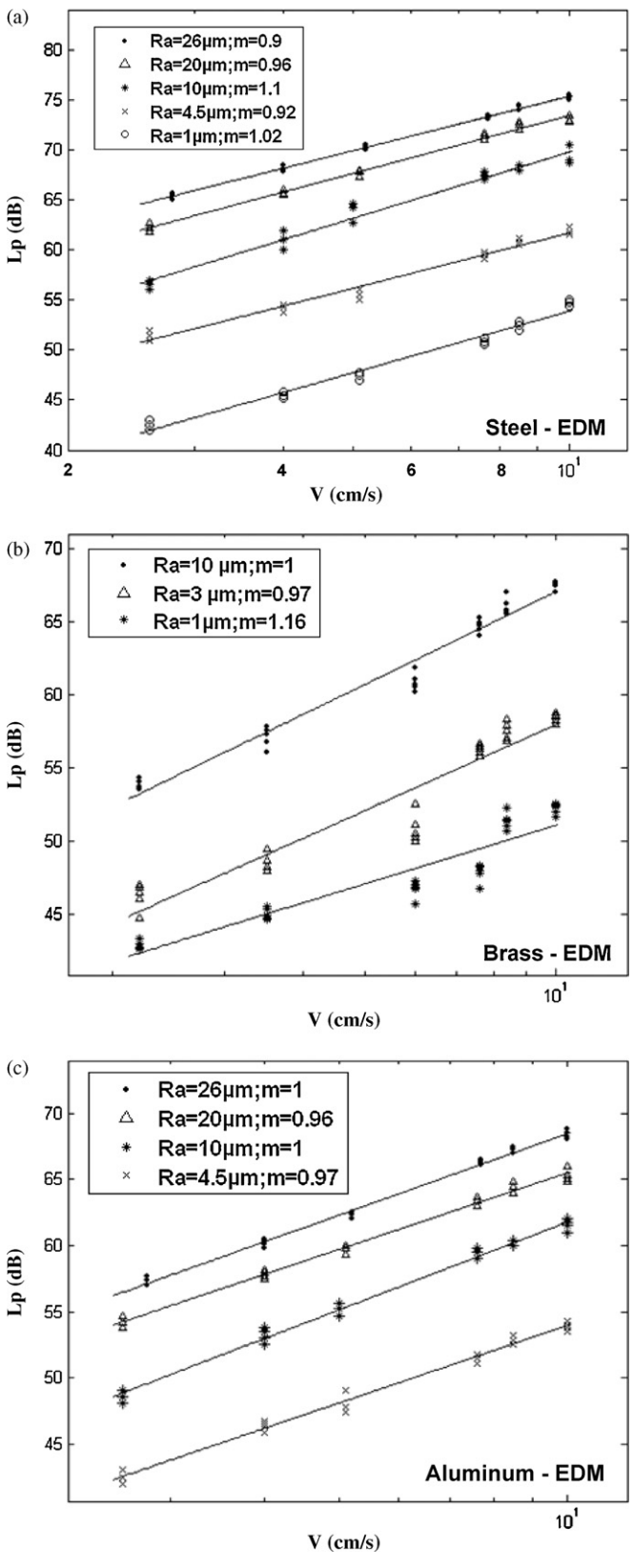

Fig. 11. Variation of the sound pressure level *Lp* (dB) versus the sliding speed, for various surface roughness obtained by EDM and different materials. (a) Steel/steel, (b) brass/brass, and (c) aluminum/aluminum.

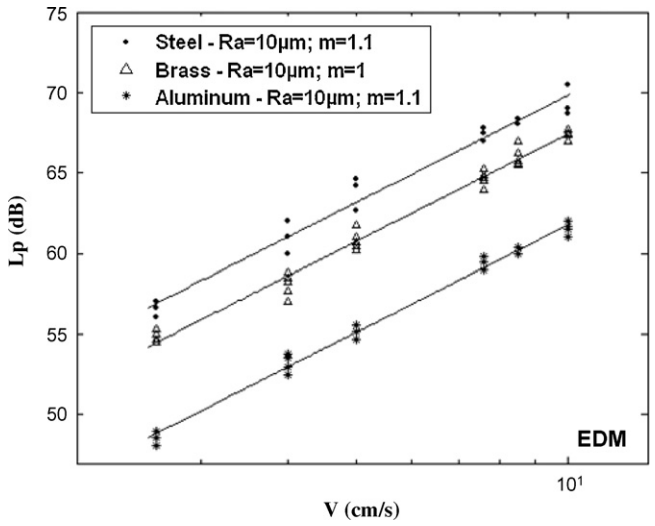

Fig. 12. Variation of the sound pressure level *Lp* (dB) versus the sliding speed, for various materials. $R_a = 10\ \mu m$.

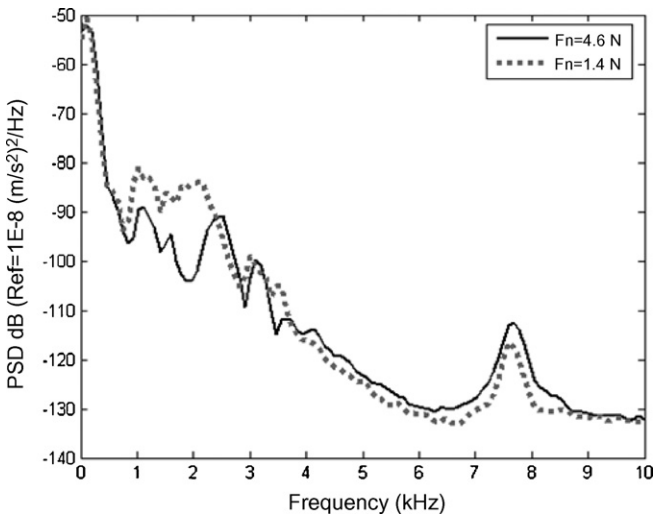

Fig. 14. Power spectrum density of roughness noise for different loading forces. Flat–flat contact, $R_a = 26\ \mu m$ (by EDM) and $V = 6$ cm/s.

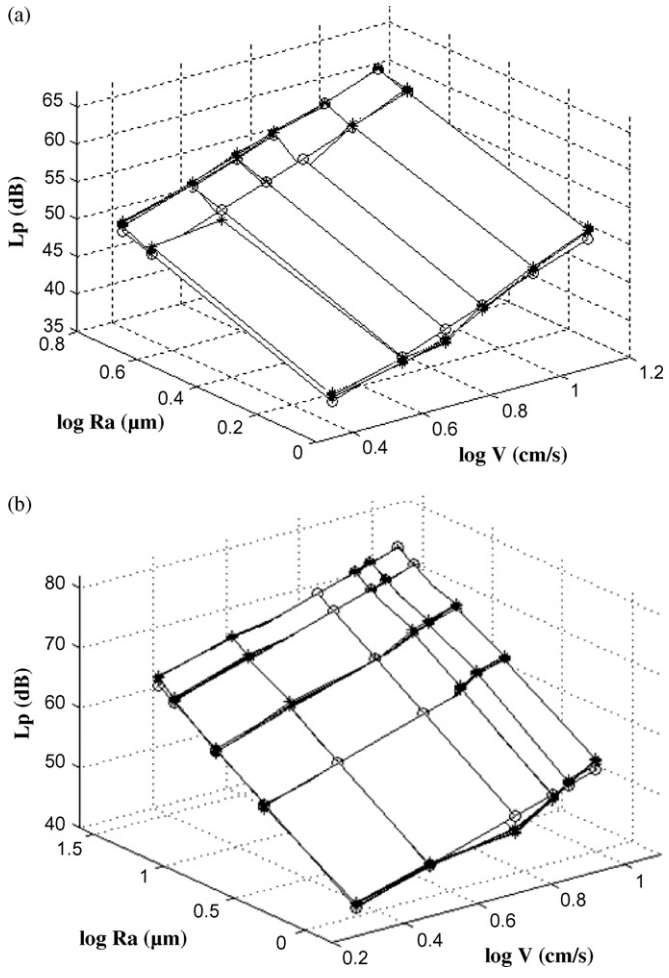

Fig. 13. Variation of the sound pressure level *Lp* (dB) versus the surface roughness and the sliding speed, (a) sandblasting, (b) EDM. (*) Experimental data, (◯) fitted data.

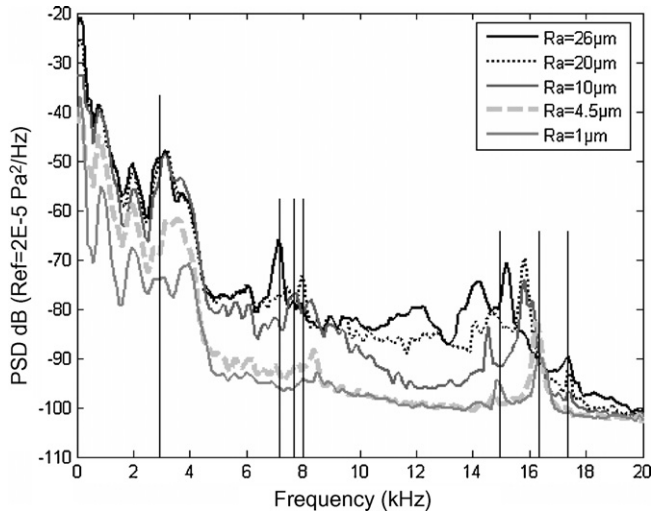

Fig. 15. Power spectrum density of roughness noise for different roughnesses. The vertical thick lines point out the position of eigenfrequencies of uncoupled samples computed by finite element method.

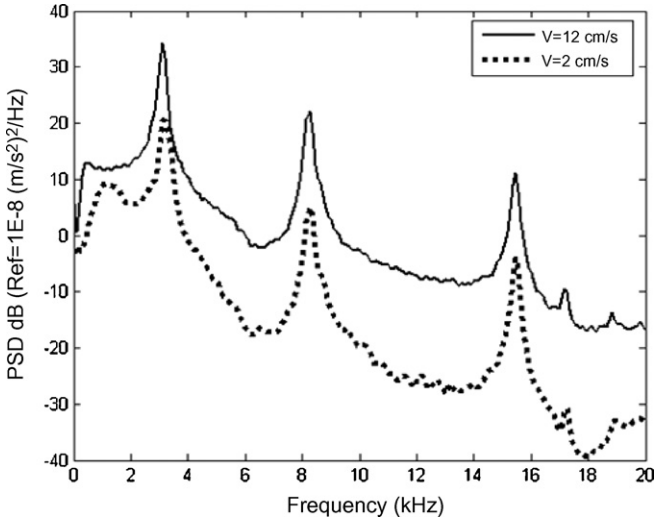

Fig. 16. Power spectrum density of roughness noise for different sliding speeds. Flat–flat contact and $R_a = 26\ \mu m$ (by EDM).

Table 9
Frequency shift of the first eigenmode, experimental contact stiffness K_{exp} (N/m) and deformation F_n/K (μm) for R_a = 1 μm, 4.5 μm, 10 μm, 20 μm and 26 μm (EDM).

	R_a (μm) (by EDM)				
	1	4.5	10	20	26
$\Delta\omega/\omega$	0.37	0.22	0.21	0.1	0.02
K_{exp} (N/μm)	22	13	12	6	2
$M\omega_i^2$ (N/μm)	112	112	112	112	112
F_n/K (μm)	0.06	0.11	0.12	0.25	0.75

2.4 kHz at R_z = 12.4 μm to 5.4 kHz at R_z = 0.8 μm. But, they do not give an explication for the origin of the shift.

Othman et al. [18] conclude that the filtered sound signal have a peak at a specific frequency ("dominating frequency") which depends on the material under investigation regardless of the surface roughness and the contact load.

Nakai and Yokoi [15] found that the largest peak of the frictional sound spectrum coincides with the fundamental natural frequency of pin. But, they do not observed any shift of peak frequencies in function of surface roughness or sliding speed.

In order to understand the shift of eigenfrequency, let consider that the interaction may be modelled as a single contact stiffness localized in the centre of the pieces. The presence of this additional stiffness acts as a constraint and then results in an increase of eigenfrequency.

Mode 1 is more dependant on the coupling strength than modes 2, 3 (which are almost one in Figs. 14–16), 4, 5, 6 and 7. This phenomenon can be explained from the numerical modal analysis. Mode 1 is a flexural one and has a maximum of vibration at the centre of the sample. This eigenfrequency therefore depends on the contact stiffness. On the other hand, all the other modes (2, 3, 4, 5, 6 and 7) have a node of vibration at the centre of the piece in normal direction. They are thus unaffected by the application of an additional rigidity (contact stiffness) at this point.

This explains why these eigenfrequencies are not dependant on the contact condition. It is apparent from Figs. 14–16 that the contact stiffness increases with the static normal load, with the reciprocal of roughness and with the reciprocal of sliding speed.

The frequency shift of the first eigenmode $\Delta\omega/\omega$ and the contact stiffness K_{exp} (N/m) for the various roughnesses are shown in Table 9.

4. Discussion and comments

Consider two identical and rough solids B_1 and B_2, in sliding contact with a relative sliding speed V. A_a and A_r are respectively the apparent and the real contact area. F_n and F_t are the applied normal load and the tangential friction force. m_1 and m_2 are respectively the masses of the solids B_1 and B_2. When the rough surfaces are rubbed together, under light load, a roughness noise is radiated. Contrary to the noise due to mechanical instabilities such as squeal, attributed to stick-slip, sprag-slip, negative friction-velocity slope, modal coupling mechanisms [23], plowing and adhesion between two sliding surfaces [24,25], roughness noise generation may be attributed to the multiples impacts between antagonist asperities.

During impacts, the contact loads in interface deform elastically the asperities in contact. After impact, the deformed asperities turn back to their stable positions. The jumps among metastable positions generate vibrations in the two solids in contact whose a share is radiated in the acoustic energy form. Three fundamental steps are involved in roughness noise phenomenon.

- Step 1 (tribology): the vibrations are generated by the variations of the contact loads and amplified by the elastic deformation of the antagonist asperities.
- Step 2 (dynamics): waves propagate through the solids. This phenomenon is driven by eigenmodes and damping of the solids.
- Step 3 (acoustics): the sound is radiated by the solid surfaces and then propagates through air to ears.

Table 10
Impact duration estimated from the roughness noise spectrum (Fig. 15) for different surface roughness.

	R_a (μm)				
	1	4.5	10	20	26
τ (ms)	0.25	0.281	0.283	0.311	0.336

It should be understood that the level Lp (dB) of the roughness noise is controlled simultaneously by the detailed topography of the surfaces in contact and the sliding speed, but also by the dynamics of the surfaces.

Thus, in terms of topography and sliding speed, it is shown that the sound pressure level Lp (dB) is simultaneously proportional to the surface roughness and the sliding speed (Fig. 13) regardless of the material under investigation, the contact geometry and the samples machining process.

In terms of dynamics, when the rough surfaces are rubbed together, the contact has its own stiffness K which results from the superposition of all contact spots. This contact stiffness depends on all contact conditions and, in particular it is an increasing function of the contact pressure [22] which is low in the case of roughness noise.

This condition makes that the contact stiffness K is low, and as a result the coupling between the two samples is light and they behave like being totally uncoupled (Table 9):

$$K \ll M\omega_i^2 \tag{7}$$

where M is the mass of solids and ω_I (rad/s) are the eigenfrequencies of isolated solids. This shows that the natural modes are stiffer than the contact. This explains why the modes of isolated solids are not significantly affected by the application of an additional rigidity (contact stiffness). But when the roughness decreases (Fig. 15), the coupling become more important and the first eigenfrequency is shifted towards high frequencies (Table 9).

It is known that for very rough surfaces, sliding contact causes a deformation of asperities surfaces [22,26]. However, in the case of roughness noise, the deformation of surfaces during contact is very light and its magnitude is negligible compared to the surface roughness (Table 9).

$$\delta = \frac{F_n}{K} \ll R_a \tag{8}$$

Therefore, the contact appears on the tops of asperities surfaces. The underlying physics involves the so-called multi-contact interfaces [22,26,27]. In this configuration, the real contact area A_r is a small part of the apparent contact area A_a.

The duration τ of impacts occurring between the antagonist asperities surfaces, during sliding contact, can be estimated from the frequencies spectrum of roughness noise (Fig. 15):

$$\tau = \frac{1}{f_1} \tag{9}$$

where f_1 (Hz) is the natural frequency of the first eigenmode. Table 10 shows the impact duration estimated from the roughness noise spectrum presented in Fig. 15. It is clear that the impact duration is an increasing function of the surface roughness. This can be explained by the peak shift in the roughness noise spectrum towards high frequencies when the surface roughness decreases.

5. Conclusion

It is concluded that for sliding rough surfaces under light load the fundamental mechanism of radiated noise, called roughness noise, is attributed to the multiples impacts between antagonist asperities of sliding surfaces. The jumps between metastable positions of surface asperities are the most important source of energy dissipation whose a share is radiated in the acoustic energy form.

Three fundamental steps are involved in roughness noise phenomenon: tribology (vibrations are generated by the variations of the contact loads in the interface), dynamics (propagation of the vibrations in the solids in contact) and acoustics (roughness noise is radiated by the solid surfaces).

It is shown that the sound pressure level Lp (dB) of the roughness noise is controlled simultaneously by the detailed topography of the surfaces in contact, the sliding speed and the dynamics of the surfaces.

In terms of topography and sliding speed, it was shown that the roughness noise is simultaneously an increasing linear function of the logarithm of the surface roughness and the sliding speed. The exponents n and m are independents and they are respectively $0.7 \leq n \leq 0.96$ and $0.8 \leq m \leq 1.16$.

In terms of dynamics, it was shown that, roughness noise is generated for light dynamical coupling. Under this condition, the natural modes of samples are stiffer than the contact and therefore the resulting vibrations are not affected by the additional rigidity. The deformation of surfaces during contact is very light and its magnitude is negligible compared to the surface roughness.

References

[1] H. Zahouani, R. Vargiolu, J.L. Loubet, Fractal models of surface topography and contact mechanics, Math. Comput. Modell. 28 (4–8) (1998) 517–534.
[2] H. Zahouani, F. Sidoroff, Rough surfaces and elasto-plastic contacts, C. R. Acad. Sci. Paris, t.2, Série IV (2001) 709–715.
[3] H. Zahouani, M. Assoul, R. Vargiolu, T. Mathia, The morphological tree transform of surface motifs. Incidence in tribology, Int. J. Mach. Tools Manuf. 41 (2001) 1961–1979.
[4] J. Jamari, D.J. Schipper, Deformation due to contact between a rough surface and a smooth ball, Wear 262 (2007) 138–145.
[5] D. Sinclair, Frictional vibrations, J. Appl. Mech. (1955) 207–214.
[6] C.A. Brockley, R. Cameron, A.F. Potter, Friction-induced vibration, J. Lubr. Technol. (1967) 101–108.
[7] D.P. Hess, A. Soom, Normal vibrations and friction under harmonic loads. Part II—rough planar contacts, J. Tribol. 113 (1991) 87–92.
[8] M.O. Othman, T.W. Abou-Arab, M.C. Mirzaa, A.H. Elkholy, Friction-induced vibrations of reciprocating contacts, Tribol. Int. 28 (5) (1995) 293–300.
[9] J. Slavic, M.D. Bryant, M. Boltezar, A new approach to roughness-induced vibrations on a slider, J. Sound Vib. 306 (2007) 732–750.
[10] K. Takashi, The friction noise under heavy load, Bull. FAC. Sci. Eng. 16 (1973) 53–69 (Chuo University).
[11] M. Yokoi, M. Nakai, A fundamental study on frictional noise (1st report, the generating mechanism of rubbing noise and squeal noise), Bull. JSME 22 (1979) 1665–1671.
[12] M. Yokoi, M. Nakai, A fundamental study on frictional noise (2nd report, the generating mechanism of squeal noise of higher modes), Bull. JSME 23 (1980) 2118–2124.
[13] M. Yokoi, M. Nakai, A fundamental study on frictional noise (3rd report, the influence of periodic surface roughness on frictional noise), Bull. JSME 24 (1981) 1470–1476.
[14] M. Yokoi, M. Nakai, A fundamental study on frictional noise (4th report, the influence of angle of inclination of the rod on frictional noise), Bull. JSME 24 (1981) 1477–1483.
[15] M. Nakai, M. Yokoi, A fundamental study on frictional noise (5th report, the influence of random surface roughness on frictional noise), Bull. JSME 25 (1982) 827–833.
[16] M. Nakai, M. Yokoi, Generation mechanism of friction noises in dry friction, Jpn. J. Tribol. 35 (1990) 513–522.
[17] M.O. Othman, A.H. Elkholy, Surfaces roughness measuring using dry friction noise, Exp. Mech. 47 (1990) 309–312.
[18] M.O. Othman, A.H. Elkholy, A.A. Seireg, Experimental investigation of frictional noise and surface-roughness characteristics, Exp. Mech. 47 (1990) 328–331.
[19] T. Jibiki, M. Shima, H. Akita, M. Tamura, A basic study of friction noise caused by fretting, Wear 251 (2001) 1492–1503.
[20] A. Akay, Acoustics of friction, J. Acoust. Soc. Am. 111 (2002) 1525–1548.
[21] B.L. Stoimenov, S. Maruyama, K. Adashi, K. Kato, The roughness effect on the frequency of frictional sound, Tribol. Int. 40 (2007) 659–664.
[22] J.A. Greenwood, J.B.P. Williamson, Contact of nominally flat surfaces, Proc. R. Soc. Lond. Ser. A 295 (1966) 300–319.
[23] R.A. Ibrahim, Friction-induced vibration, chatter, squeal, and chaos. Part 2. Dynamics and modelling, Appl. Mech. Rev. 47 (1994) 227–252.
[24] N.P. Suh, H.C. Sin, The genesis of friction, Wear 69 (1981) 91–114.
[25] C. Guangxiong, Z. Zhongrong, P. Kapsa, L. Vincent, Effect of surface topography on formation of squeal under reciprocating sliding, Wear 253 (2002) 411–423.
[26] J.F. Archard, Elastic deformation and the laws of friction, Proc. R. Soc. Lond. Ser. A 243 (1957) 190–205.
[27] F.P. Bowden, D. Tabor, The Friction and Lubrication of Solids I, Clarendon Press, Oxford, 1950.